SCIENTIFIC REPORTS

OPEN

SUBJECT AREAS:
BIOENERGETICS
BIOPHYSICAL CHEMISTRY

Received
25 July 2014

Accepted
10 February 2015

Published
6 March 2015

Correspondence and requests for materials should be addressed to P.P. (pavel.pospisil@upol.cz)

The formation of electronically excited species in the human multiple myeloma cell suspension

Marek Rác[1], Michaela Sedlářová[2] & Pavel Pospíšil[1]

[1]Department of Biophysics, Centre of the Region Haná for Biotechnological and Agricultural Research, Faculty of Science, Palacký University, Šlechtitelů 11, 783 71 Olomouc, Czech Republic, [2]Department of Botany, Faculty of Science, Palacký University, Šlechtitelů 11, 783 71 Olomouc, Czech Republic.

In this study, evidence is provided on the formation of electronically excited species in human multiple myeloma cells U266 in the growth medium exposed to hydrogen peroxide (H_2O_2). Two-dimensional imaging of ultra-weak photon emission using highly sensitive charge coupled device camera revealed that the addition of H_2O_2 to cell suspension caused the formation of triplet excited carbonyls $^3(R = O)^*$. The kinetics of $^3(R = O)^*$ formation in the real time, as measured by one-dimensional ultra-weak photon emission using low-noise photomultiplier, showed immediate enhancement followed by a slow decay. In parallel to the formation of $^3(R = O)^*$, the formation of singlet oxygen ($^1O_2$) in U266 cells caused by the addition of H_2O_2 was visualized by the imaging of $^1O_2$ using the green fluorescence of singlet oxygen sensor green detected by confocal laser scanning microscopy. Additionally, the formation of $^1O_2$ after the addition of H_2O_2 to cell suspension was detected by electron paramagnetic resonance spin-trapping spectroscopy using 2,2,6,6-tetramethyl-4-piperidone. Presented results indicate that the addition of H_2O_2 to cell suspension results in the formation of $^3(R = O)^*$ and $^1O_2$ in U266 cell suspension. The contribution of the cell-free medium to the formation of electronically excited species was discussed.

Reactive oxygen species (ROS) are produced as a byproduct of either metabolic processes such as cellular respiration in mitochondria and photosynthesis in chloroplast[1–3] or oxidative burst in phagocytic cells known to play role in the defense against infection[4]. The one-electron reduction of molecular oxygen produces superoxide anion radical ($O_2^{\bullet-}$) known to dismutate to hydrogen peroxide (H_2O_2) and subsequently to hydroxyl radical ($HO^{\bullet}$). When ROS are not sufficiently eliminated by non-enzymatic (low molecular weight scavengers) and enzymatic (the superoxide dismutase and peroxidase families of enzymes) defense systems, ROS oxidize biomolecules comprising lipid, protein and nucleic acid[5–8]. The oxidation of lipid and protein by abstraction of weakly bonded hydrogen atom by $HO^{\bullet}$ results in the formation of lipid and protein alkyl radicals ($R^{\bullet}$), respectively. Subsequently, lipid and protein peroxyl radicals ($ROO^{\bullet}$) are formed by the interaction of $R^{\bullet}$ with molecular oxygen. Peroxyl radicals abstract hydrogen from lipid and protein, while lipid and protein hydroperoxides (ROOH) are formed. Under reducing conditions (reduced transition metals such as Fe^{2+}, Mn^{2+}, Zn^{2+} or Cu^{+} bound in metalloproteins, transport proteins, and storage proteins), ROOH is reduced to lipid and protein alkoxyl radicals ($RO^{\bullet}$), whereas under oxidizing conditions (oxidized transition metals, cytochrome c, peroxynitrite, chloroperoxide, and hypochlorous acid), ROOH is oxidized back to lipid and protein $ROO^{\bullet}$[9,10].

The oxidation of biomolecules by ROS was proposed to be associated with the formation of electronically excited species such as triplet excited carbonyl $^3(R = O)^*$ and singlet oxygen ($^1O_2$)[11–14]. Based on chemical system experiments, $^3(R = O)^*$ was proposed to be produced by the decomposition of cyclic (1,2-dioxetane, ROOR) and linear (tetroxide, ROOOOR) high-energy intermediates. 1,2-dioxetane is formed by the cycloaddition of $^1O_2$ to lipid and protein, by the cyclization of lipid and protein $ROO^{\bullet}$[15], and by the enzymatic reactions[16–18]. Tetroxide is formed by the recombination of two lipid and protein $ROO^{\bullet}$ via Russell mechanism[15,19]. Once $^3(R = O)^*$ is formed, the excitation energy of $^3(R = O)^*$ can be transferred either to molecular oxygen resulting in the formation of $^1O_2$[20] or to chromophore (C) forming singlet excited chromophore ($^1C^*$)[14]. Beside the reactions related to the transfer of excitation energy, $^3(R = O)^*$ is known to undergo a variety of other reactions comprising of isomerization, cleavage, hydrogen abstraction, and cycloaddition[21,22]. In addition to $^3(R = O)^*$ pathway, the direct decomposition of ROOOOR to $^1O_2$ by Russell mechanisms was evidenced in the chemical system[23,24]. More recently, several lines of evidence were provided on the formation of $^1O_2$ by the decomposition of lipid and protein ROOH by metal ions, cytochrome c, peroxynitrite, chloroperoxide, and hypochlorous acid[25–28]. As the yield of $^3(R$

= O)* formation during the decomposition of ROOOOR was found to be 10^3–10^4 lower compared to the yield of $^1O_2$ formation, it was proposed that the Russell mechanism leads predominantly to the formation of $^1O_2$, whereas the formation of ^{3}(R = O)* is rather negligible[29].

The excitation energy of electronically excited species formed under oxidative processes is emitted as ultra-weak photon emission[14,30–32]. The excitation energy of ^{3}(R = O)* is emitted as near UVA and blue-green photons in the spectral range of 350–550 nm[14,19]. The photon emission of ^{1}C* is in the green-red region of the spectrum (550–750 nm)[14], whereas dimol and monomol photon emission of $^1O_2$ is in the red (634, 703 nm) and infra-red (1270 nm) region of the spectrum[33,34], respectively. Recent development in one-dimensional detection of ultra-weak photon emission using low-noise photomultiplier tubes (PMT) and two-dimensional detection of ultra-weak photon emission using highly sensitive charge coupled device (CCD) cameras allows temporal and spatial visualization of the formation of electronically excited species.

In spite of the fact that several lines of evidence were provided on the formation of ^{3}(R = O)* and $^1O_2$ in chemical system, a limited number of studies have focused on the production of electronically excited species in cells. In this study, experimental evidence on the formation of ^{3}(R = O)* and $^1O_2$ in human multiple myeloma cell line U266 suspended in the growth medium containing free amino acids, fetal bovine serum and traces of transition metal ions is provided. The detection of the electronically excited species was performed using ultra-weak photon emission, confocal laser scanning microscopy and electron paramagnetic (EPR) spin-trapping spectroscopy. It is demonstrated here that both ^{3}(R = O)* and $^1O_2$ are formed in the cell suspension exposed to oxidative environment.

Results

The effect of various H_2O_2 concentrations on the formation of the electronically excited species and cell viability. To select the most suitable concentration of H_2O_2 for the formation of ^{3}(R = O)* and $^1O_2$, the effect of various H_2O_2 concentrations on the formation of ^{3}(R = O)* and $^1O_2$ was tested using one-dimensional ultra-weak photon emission and EPR spin-trapping spectroscopy, respectively. Figure 1A shows the one-dimensional ultra-weak photon emission measured from cell suspension after the addition of H_2O_2 at different concentrations. The addition of H_2O_2 at different concentrations to the cell suspension resulted in the immediate significant increase of one-dimensional ultra-weak photon emission as compared to the untreated cell suspension. In further, the formation of TEMPONE EPR signal in cell suspension was measured after the addition of H_2O_2 at various concentrations. Figure 1B shows that TEMPONE EPR signal was enhanced nonlinearly with the increasing concentration of H_2O_2. These observations reveal that the addition of 5 mM H_2O_2 to the cell suspension results in sufficient response allowing the detection of electronically excited species. To test whether 5 mM H_2O_2 affects the viability of cells, the number of live cells was determined after the addition of 5 mM H_2O_2. Figure 1C shows that the cell viability remained unaffected by the addition of 5 mM H_2O_2 to the cell suspension. Based on the results from one-dimensional ultra-weak photon emission, EPR spin-trapping spectroscopy, and cell viability, the concentration of 5 mM H_2O_2 was chosen for further experiments.

The detection of triplet excited carbonyls by two-dimensional ultra-weak photon emission. To visualize the formation of ^{3}(R = O)* in cell suspension treated with H_2O_2, the two-dimensional ultra-weak photon emission was examined using a highly sensitive CCD camera. Figure 2 shows the two-dimensional ultra-weak photon emission measured from cell suspension after the addition of H_2O_2. The treatment of cell suspension with H_2O_2 resulted in the pronounced increase in two-dimensional ultra-weak photon emission compared to control. To quantify the differences in two-dimensional ultra-weak photon emission from cell suspension treated with H_2O_2, the spatial profile of photon emission in the middle strip of the image was used. The number of counts of two-dimensional ultra-weak photon

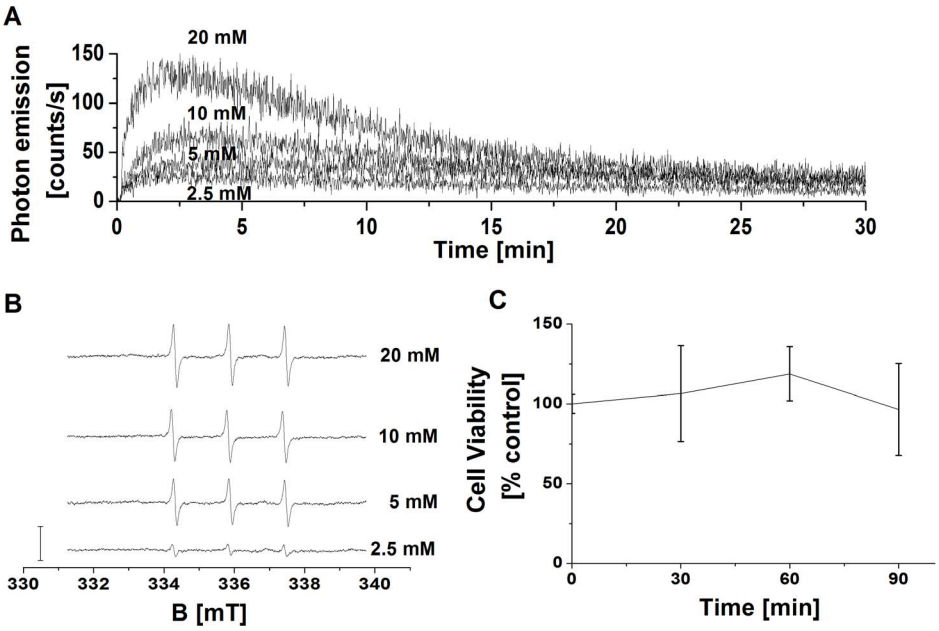

Figure 1 | The effect of various concentrations of H_2O_2 on the formation of electronically excited species. In (A), detection of one-dimensional ultra-weak photon emission. One-dimensional ultra-weak photon emission from cell suspension was measured by low-noise PMT after the addition of H_2O_2 at concentrations indicated in the figure. In (B), detection of TEMPONE EPR signal by EPR spin-trapping spectroscopy. TEMPONE EPR spectra were detected from cell suspension treated with H_2O_2 for 30 min at the concentrations indicated in the figure. 50 mM TEMPD was added to cell suspension prior to the measurement. The bar represents 3000 relative units. In (C), determination of cell viability by automated cell counter. The cell suspension was treated with 5 mM H_2O_2 for the time period indicated in the figure. The data are presented as the mean and standard deviation of 3 measurements (mean ± SD, n = 3).

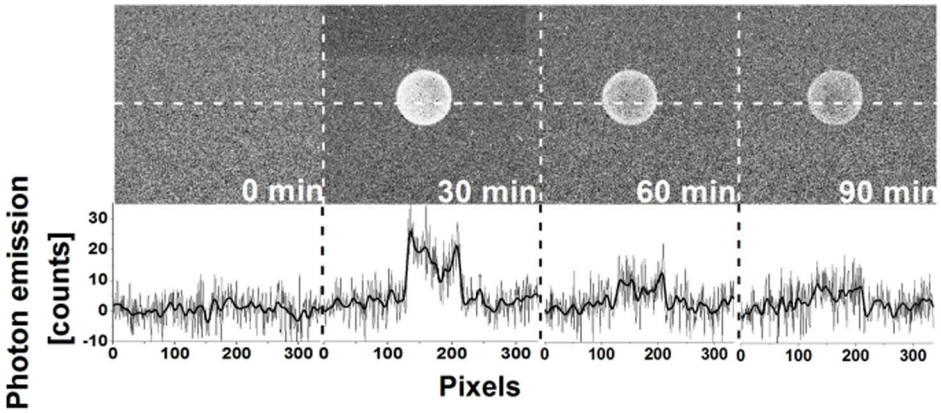

Figure 2 | Triplet excited carbonyl detection by two-dimensional imaging of ultra-weak photon emission. Two-dimensional ultra-weak photon emission was measured from the cell suspension by a highly sensitive CCD camera. Prior to the measurements, the cell suspension was kept in the dark for 10 min. After dark period, two-dimensional ultra-weak photon emission was measured from untreated cell suspension. Consequently, a set of three images of two-dimensional ultra-weak photon emission was measured after the addition of H_2O_2 to cell suspension for time period indicated in the figure. The two-dimensional ultra-weak photon emission was measured with the integration time of 30 min. The bottom panel shows the spatial profile of photon emission in the middle strip of the image. Y axis denotes the number of counts accumulated after 30 min, whereas X axis denotes the pixel of the image.

emission from cell suspension measured in the absence of H_2O_2 was under the detection limit of CCD camera. The intensity of two-dimensional ultra-weak photon emission was highest during the first 30 min. These results indicate that the addition of H_2O_2 to cell suspension causes the formation of $^3(R = O)^*$.

Detection of triplet excited carbonyls by one-dimensional ultra-weak photon emission. To study the kinetics of ultra-weak photon emission, one-dimensional ultra-weak photon emission was measured using low-noise PMT. Spontaneous one-dimensional ultra-weak photon emission from cell suspension measured in the absence of H_2O_2 shows a steady-state level, whereas the addition of H_2O_2 after 30 min induced pronounced enhancement of one-dimensional ultra-weak photon emission followed by slow decay (Fig. 3A). To confirm that one-dimensional ultra-weak photon emission is in the region of the spectrum assigned to $^3(R = O)^*$, the one-dimensional ultra-weak photon emission was measured using long-pass edge filter (600 nm). Figure 3B shows that one-dimensional ultra-weak photon emission

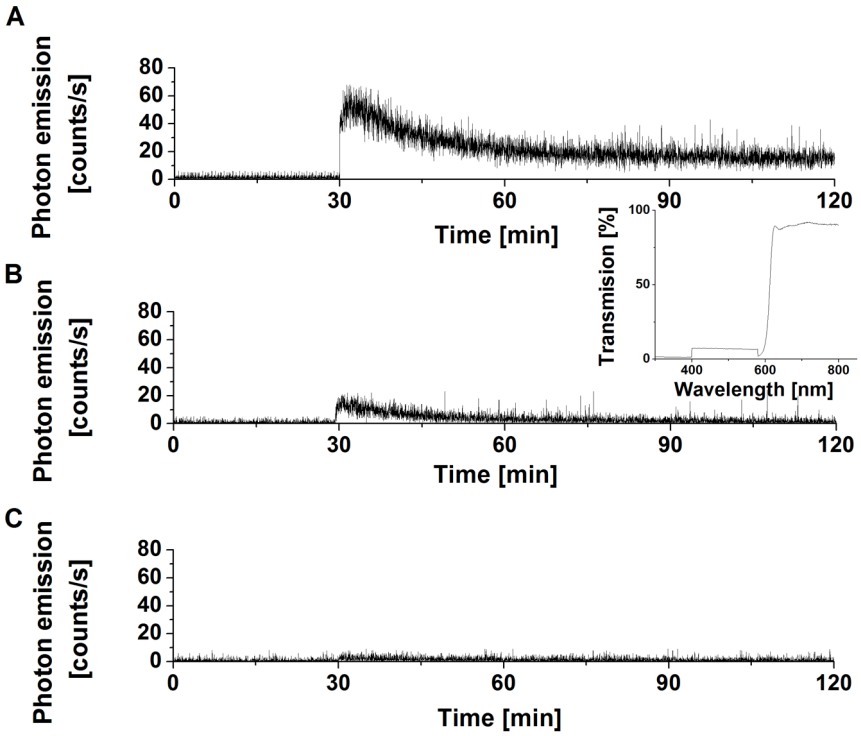

Figure 3 | Triplet excited carbonyl detection by one-dimensional ultra-weak photon emission. One-dimensional ultra-weak photon emission from cell suspension was measured by low-noise PMT. In (A), spontaneous one-dimensional ultra-weak photon emission was measured for 30 min. Consequently, 5 mM H_2O_2 was added to the cell suspension. In (B), the one-dimensional ultra-weak photon emission from cell suspension treated with 5 mM H_2O_2 was measured in the presence of the long-pass edge filter (600 nm). Insert shows transmission spectrum of long-pass edge filter. In (C), the effect of 10 mM histidine on one-dimensional ultra-weak photon emission from cell suspension is shown. Other experimental conditions were as in Fig. 2B.

was significantly suppressed in the presence of the long-pass edge filter. To determine the participation of $^1O_2$ in one-dimensional ultra-weak photon emission originated from red region of the spectrum, the effect of histidine, $^1O_2$ scavenger, on one-dimensional ultra-weak photon was measured. Figure 3C demonstrates that the one-dimensional ultra-weak photon emission in the red region was almost fully suppressed in the presence of histidine. These results prove that most of the one-dimensional ultra-weak photon emission originates from the blue-green region of the spectrum known to be associated with the photon emission of $^3(R = O)^*$. Moreover, the measurement of one-dimensional ultra-weak photon emission reveals that the formation of $^3(R = O)^*$ starts immediately after the addition of H_2O_2 to the cell suspension.

Formation of singlet oxygen detected by confocal laser scanning microscopy. To visualize the formation of $^1O_2$ in U266 cells caused by the addition of H_2O_2, singlet oxygen sensor green (SOSG) fluorescence was detected by confocal laser scanning microscopy. In spite of its high selectivity to $^1O_2$ without any undesirable interaction with $O_2^{\bullet-}$ and $HO^{\bullet}$[35], the SOSG has been reported to suffer from self-photosensitization[35]. To prevent the formation of $^1O_2$ by SOSG itself, the dye was strictly protected from light exposition during the whole experiment. Figure 4A shows the combination of channels for SOSG fluorescence (in green) and Nomarski DIC (greyscale) of U266 cells treated with H_2O_2 for 0, 30, 60 and 90 min. Negligible SOSG fluorescence detected from untreated U266 cells was due to the weak SOSG fluorescence upon excitation by light at 480 nm prior to the reaction with $^1O_2$. The formation of SOSG endoperoxide by the cycloaddition of $^1O_2$ precludes the intramolecular electron transport thus resulting in the enhancement of the fluorescence. The intensity of SOSG fluorescence was pronouncedly higher in the H_2O_2-treated U266 cells compared to untreated U266 cells. Figure 4B represents the integral distribution of SOSG fluorescence intensity within the corresponding upper image. Although SOSG was originally devised for extracellular applications, several studies reported its penetration inside of cells[36,37]. To test whether SOSG penetrates into U266 cells, SOSG fluorescence was measured in the multiple layers of sample (Fig. 5). The presence of SOSG fluorescence in the multiple layers of sample reveals the formation of $^1O_2$ inside of U266 cells after the addition of H_2O_2.

Formation of singlet oxygen detected by EPR spin-trapping spectroscopy. To study the kinetics of $^1O_2$ formation in the cell suspension, EPR spin-trapping spectroscopy was used. The spin-trapping was accomplished by utilizing the oxidation of hydrophilic diamagnetic 2,2,6,6-tetramethyl-4-piperidone (TMPD) by $^1O_2$ known to yield paramagnetic 2, 2, 6, 6-tetramethyl-4-piperidone-1-oxyl (TEMPONE). The observation that no TEMPONE EPR signal was detected in untreated cell suspension indicates that no $^1O_2$ was formed in the untreated cell suspension (Fig. 6). The addition of H_2O_2 to the cell suspension caused the formation of TEMPONE EPR signal. To confirm that EPR signal is attributed to TEMPONE, the EPR spectrum of pure TEMPONE was measured. The simulation of TEMPONE EPR spectra using one spectral component with the hyperfine coupling constant $a^N = 16$ G provided agreement with the hyperfine coupling constant described

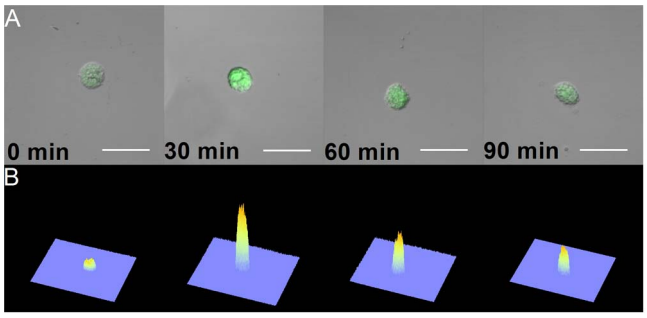

Figure 4 | Singlet oxygen imaging by confocal laser scanning microscopy. The SOSG fluorescence within U266 cells treated with 5 mM H_2O_2 for the time period indicated in the figure was examined by a confocal laser scanning microscope. 50 μM SOSG was added to U266 cells 30 min prior to the data collection. In (A), individual representative cells of each time variant are shown in the images combining Nomarski DIC and SOSG fluorescence (λ_{em} = 505–525 nm) channels. In (B), the integral distribution of the SOSG fluorescence intensity is shown within the corresponding upper images. The bar represents 30 μm.

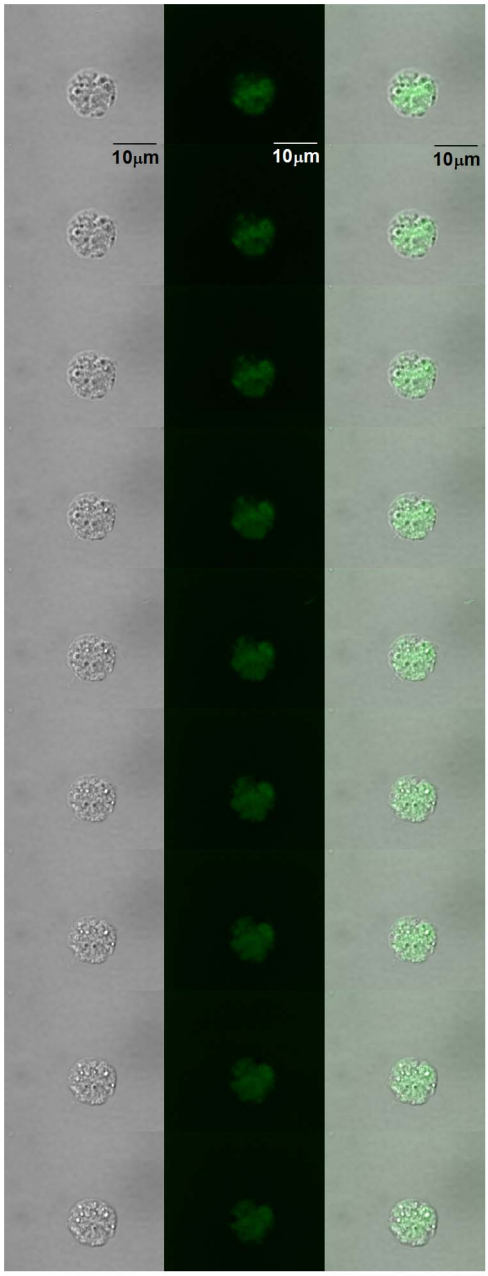

Figure 5 | Singlet oxygen imaging in the multiple layers of the sample. U266 cells were treated with 5 mM H_2O_2 for 30 min. Three channels are presented: Nomarski DIC (left column), SOSG fluorescence (λ_{em} = 505–525 nm) (middle column) and the combination of Nomarski DIC and SOSG fluorescence (right column). The step in between different pictures is 0.5 μm. Other parameters are same as in Fig. 4.

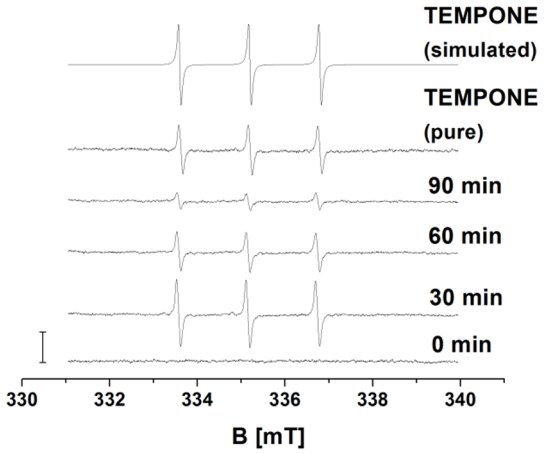

Figure 6 | Detection of singlet oxygen by EPR spin-trapping spectroscopy. TEMPONE EPR spectra were detected from cell suspension treated with 5 mM H_2O_2 for the period indicated in the figure. 50 mM TEMPD was added to cell suspension 30 min prior to the measurement. Pure TEMPONE EPR signal was detected using 20 nM TEMPONE. The simulation of TEMPONE EPR spectra was done using hyperfine splitting constant a^N = 16 G. The bar represents 3000 relative units.

for TEMPONE[38]. These results indicate that the addition of H_2O_2 to cell suspension results in the formation of $^1O_2$.

Quantitative analysis of triplet excited carbonyls and singlet oxygen formation. In order to quantify $^3(R = O)^*$ and $^1O_2$, two-dimensional ultra-weak photon emission, one-dimensional ultra-weak photon emission, SOSG fluorescence and TEMPONE EPR signal were plotted as a function of H_2O_2 treatment period. To quantify two-dimensional images of ultra-weak photon emission from cell suspension treated with H_2O_2, the aera below the curve of spatial profile of photon emission at different strips of the image was counted. The intensity of the two-dimensional ultra-weak photon emission decreased by 50% and 62% after the addition of H_2O_2 for 60 and 90 min compared to 30 min (Fig. 7A). To evaluate one-dimensional ultra-weak photon emission from cell suspension treated with H_2O_2, the area below curve was counted over the 30 min of the treatment (Fig. 7B). Two-dimensional ultra-weak photon emission measured from the cell suspension decreased by 55% and 72% after the addition of H_2O_2 for 60 and 90 min compared to 30 min. To evaluate the SOSG fluorescence obtained using confocal laser scanning microscopy, the intensity of SOSG fluorescence within confocal images was analyzed by image analysis (Fig. 7C). Due to the high background of SOSG fluorescence, the intensity of SOSG fluorescence observed in untreated U266 cells was subtracted from the SOSG fluorescence observed in treated U266 cells prior to the evaluation. The SOSG fluorescence was decreased by 50% and 80% after the addition of H_2O_2 for 60 and 90 min compared to 30 min. The plotting of the height of the center peak of TEMPONE EPR spectrum against the time showed that TEMPONE EPR signal decreased by 50% and 75% after the addition of H_2O_2 for 60 and 90 min compared to 30 min (Fig. 7D). These results show that the formation of both $^3(R = O)^*$ and $^1O_2$ decays rapidly shortly after the addition of H_2O_2 to cell suspension followed by slow decay over the whole time of experiment.

The involvement of the medium in the formation of electronically excited species. In order to evaluate the effect of the medium on the formation of electronically excited species, the cell suspension was gently centrifuged and the supernatant was taken for further experiments. The addition of H_2O_2 to both cell suspension and cell-free medium resulted in significant increase in both the one-dimensional ultra-weak photon emission and TEMPONE EPR signal. The comparison of results revealed that the one-dimensional ultra-weak photon emission originated from the cell-free medium was lower by

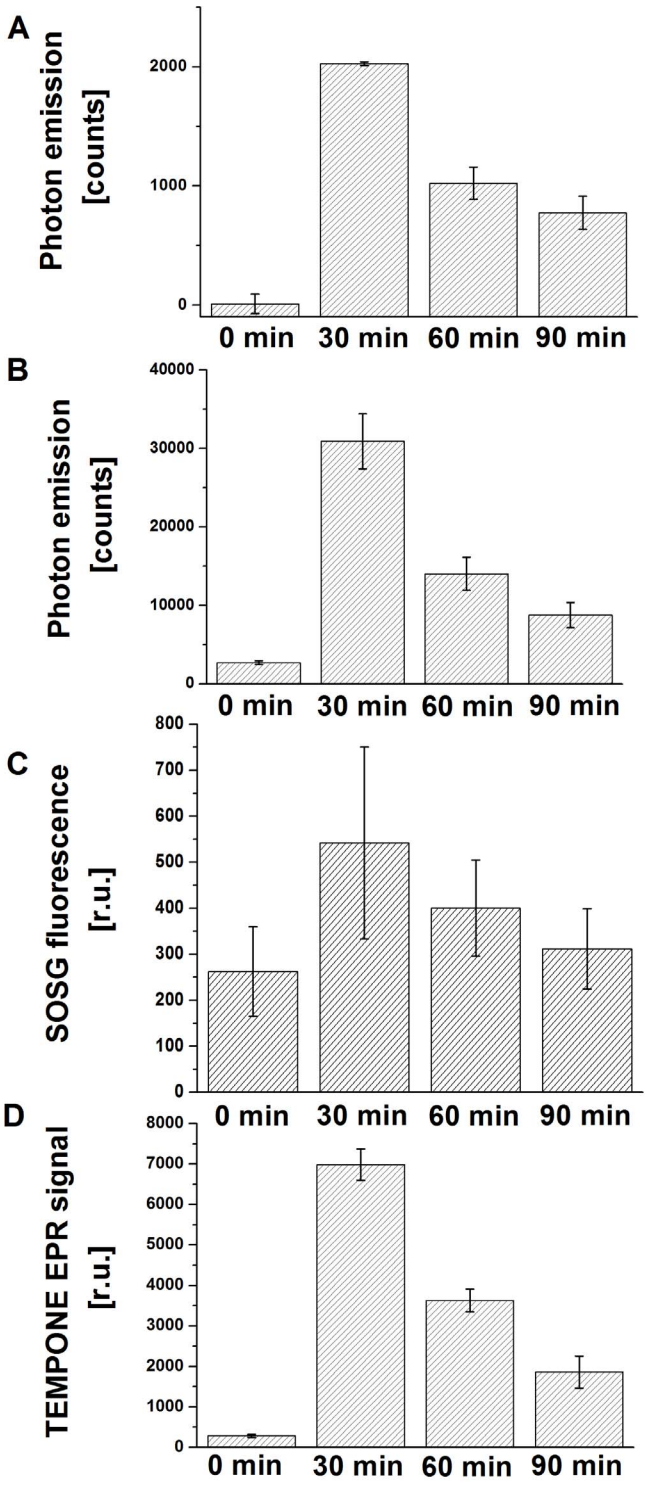

Figure 7 | Quantitative analysis. Quantitative analysis of two-dimensional and one-dimensional ultra-weak photon emission, SOSG fluorescence intensity, and TEMPONE EPR signal. The spatial profile of ultra-weak photon emission in the middle trip of the image (A), the area below curve (B), the intensity of SOSG fluorescence (C) and the height of the middle peak of TEPONE EPR signal (D) measured from U266 cells was plotted as a function of the H_2O_2 treatment period indicated in the figure. The data are presented as the mean and standard deviation of at least 3 measurements (mean ± SD, n ≥ 3). The other experimental conditions were as in Figs. 1–4.

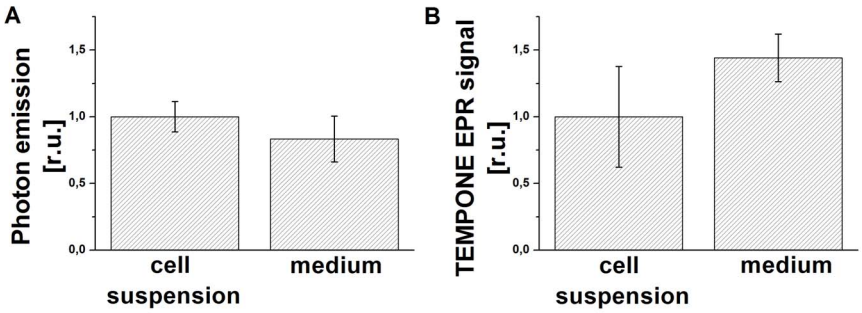

Figure 8 | Formation of electronically excited species in the cell-free medium. The one-dimensional ultra-weak photon emission (A) and TEMPONE EPR signal (B) detected in the cell suspension and in the cell-free medium 30 min after the addition of 5 mM H_2O_2 is shown. In order to better compare the results, the sum of one-dimensional ultra-weak photon emission counts and the height of the middle peak of TEPONE EPR signal were normalized to the data from cell suspension.

17% compared to the cell suspension (Fig. 8A). On the other hand, the TEMPONE EPR signal detected from cell-free medium treated with H_2O_2 was higher by 44% compared to the TEMPONE EPR signal detected from cell suspension treated with H_2O_2 (Fig. 8B). These results suggest that the contribution of the cell-free medium to the formation of electronically excited species is not negligible.

Discussion

Two-dimensional ultra-weak photon emission confirms the formation of $^3(R = O)^*$ upon the addition of H_2O_2 to cell suspension. Based on the results obtained by one-dimensional ultra-weak photon emission, it is concluded here that the formation of $^3(R = O)^*$ occurs immediately after the addition of H_2O_2 to cell suspension. Spectral analysis of the ultra-weak photon emission from different samples such as rat perfused lung, rat brain and liver homogenate, spinach mitochondria, cotyledons of etiolated seedlings of *Cicer arietinum* L., DNA, hemodialysis plasma cells, esophageal carcinoma cell line, porcine ex-vivo skin model induced by different treatment, showed that ultra-weak photon emission originates mostly from $^3(R = O)^*$[14,43–48]. Several lines of evidence have been provided that $^3(R = O)^*$ is formed by decomposition of ROOR or ROOOOR[11,13]. The decomposition of ROOR involves the cleavage of oxygen-oxygen and carbon-carbon bonds by two different mechanisms. The concerted mechanism involves the simultaneous cleavage of oxygen-oxygen and carbon-carbon bonds. The diradical mechanism is a two-step reaction involving the cleavage of oxygen bound prior to the cleavage of carbon-carbon bond[15]. Tetroxide is formed by the recombination of two ROO$^\bullet$. It has been demonstrated that t-butyl hydroperoxide does not participate in the ROOOOR formation due to the fact that the presence of α-hydrogen is required in order to undergo the Russell pathway[24,49]. Based on this observation, it was established that solely the primary and secondary ROO$^\bullet$ are involved in the ROOOOR formation, whereas the tertiary ROO$^\bullet$ undergoes propagation of lipid peroxidation and protein oxidation. The conditions required for the Russell mechanism makes it rather unlikely, but not impossible, to occur in biological system.

Figure 9 | Picture of U266 cells in Nomarski DIC channel.

Based on the data obtained from EPR spin-trapping spectroscopy itis concluded here that the formation of $^1O_2$ occurs after the addition of H_2O_2 to cell suspension. The visualization of $^1O_2$ formation in the multiple layers of sample confirmed that $^1O_2$ was produced inside the U266 cells. These results clearly show that U266 cells are oxidized upon the exposure of cell suspension to H_2O_2 resulting in $^1O_2$ formation. It has been previously demonstrated in the chemical systems that $^1O_2$ is formed by the decomposition of organic hydroperoxides such as linoleic acid hydroperoxides, thymidine hydroperoxides, t-butyl hydroperoxides[9,50–52]. The decomposition of linoleic acid hydroperoxide formed by the photooxidation using methylene blue has been shown to result in the formation of $^1O_2$ as confirmed by chemical trapping and monomol photon emission in near infra-red region[27]. The decomposition of ROOH results in the formation of ROO$^\bullet$ which leads to the formation of unstable ROOOOR known to decompose to $^1O_2$, R = O, and ROH via the Russell mechanism[23]. The experimental evidence indicates that $^1O_2$ is generated at a yield close to 10% by the Russell mechanism[52]. Furthermore, $^3(R = O)^*$ formed either through ROOR or ROOOOR pathway can transfer the excitation energy to molecular oxygen resulting in the formation of $^1O_2$. Other possible pathways for $^1O_2$ formation comprising the base-catalyzed reactions of H_2O_2, reaction of peroxynitrites with H_2O_2, reaction of H_2O_2 with hypochloride, and reactions involving enzymes (peroxidases and oxygenases) cannot be excluded.

The comparison of the formation of electronically excited species in the cell suspension and in the cell-free medium revealed that the addition of H_2O_2 to the cell suspension resulted in the higher formation of $^3(R = O)^*$ and the lower formation of $^1O_2$ as compared to the cell-free medium. These observations reveal that most of $^3(R = O)^*$ is formed in the cell-free medium, while the presence of the cells in the cell suspension results in the increase of $^3(R = O)^*$ formation. The decrease of $^1O_2$ formation caused by the presence of the cells in the cell suspension can be caused by two reasons. Firstly, due to the limited penetration of TMPD to the cells, the detection of $^1O_2$ formed deep inside the cells is less likely. Secondly, the cell-free medium is more suitable environment for the reactions such as Russell mechanism know to result in the formation of $^1O_2$. Based on this consideration, it is proposed that in the presence of cells the radicals formed in the medium oxidize the cellular components and thus less likely participate in $^1O_2$ formation reactions.

In conclusion, the addition of H_2O_2 to the cell suspension results in the formation of electronically excited species by three simultaneous reactions: the oxidation of cellular components[39–42], the oxidation of growth medium components, especially free amino acids and fetal bovine serum, which might further cause the oxidation of the cellular components, and the oxidation of the medium components.

In this study, we mainly focused on the detection of electronically excited species and possible explanation of their formation rather than the place of their origin. The detail characterization of the site of origin of the electronically excited species will be the subject of the forthcoming study.

Methods

Cell Culture. Human MM cell line U266 was used in this study[53] (Fig. 9). U266 cells were grown in RPMI-1640 supplemented with 2 mM L-glutamine, 10% FBS, antibiotics at 37°C in humidified 5% CO_2 atmosphere. Viability of the cells was measured by Trypan Blue viability test. Subsequently, 10 µl of cell suspension was mixed with 10 µl of 0.4% Trypan Blue. Cells were counted by TC20 automated cell counter (Bio-Rad Laboratories, California, USA).

Two-dimensional ultra-weak photon emission imaging. Two-dimensional ultra-weak photon emission was detected by CCD camera installed in a temperature controlled black box placed in a black painted inner darkroom. The measurement systems inside the inner darkroom were controlled and data were recorded with the computer located in the outer darkroom. The highly sensitive CCD camera VersArray 1300B (Princeton instruments, Trenton, NJ, USA) with spectral sensitivity in the range 350 to 1000 nm and close to 90% quantum efficiency in the visible range of the spectra was used to record the 2-D spectra. Objective lens of 50 mm focal distance (F mount Nikkor 50-mm, f: 1,2, Nikon) was used to enhance the light collecting efficiency. The CCD element was cooled down to −110°C in order to reduce the dark count. The following parameters were used during the measurement: scan rate 100 kHz; gain 2; image format 1340 × 1300 pixels; binning mode 4; distance between detector and the reflecting mirror 40 cm; and accumulation time 30 min.

One-dimensional ultra-weak photon emission. One-dimensional ultra-weak photon emission was detected by PMT system installed in a black painted inner darkroom. The measurement systems inside the inner darkroom were controlled and data were recorded with the computer located in the outer darkroom. A low-noice PMT R7518P, sensitive in the spectral range 185 to 730 nm, and a photon counting unit C9744 (Hamamatsu Photonics K.K., Iwata City, Japan) were employed to measure one-dimensional photon emission. To reduce the dark noise, PMT was cooled down to −30°C using thermoelectric cooler C9143 (Hamamatsu Photonics, K.K., Iwata City, Japan). All the measurements were recorded at −960 mV. The PMT was placed 5 cm above the sample during the measurement. In order to cut off the blue-green region of the spectra long-pass edge interference filter (600 nm) was used.

Detection of singlet oxygen by electron paramagnetic resonance spin-trapping spectroscopy. EPR spin-trapping spectroscopy was used to monitor the formation of $^1O_2$ in cell suspension. Hydrophilic compound TMPD was used in order to detect $^1O_2$. To eliminate the impurity of TMPD EPR signal, the TMPD was purified twice by vacuum distillation. Cell suspension was treated with 5 mM H_2O_2 in the presence of 50 mM TMPD and culture medium. Cell suspension previously treated with H_2O_2 were put into a glass capillary tube (Blaubrand intraMARK, Brand, Germany) and EPR spectra were recorded using an EPR spectrometer MiniScope MS400 (Magnetechh GmbH, Berlin, Germany). EPR conditions were as follows: microwave power, 10 mW; modulation amplitude, 1 G; modulation frequency, 100 kHz, sweep width, 100 G, scan rate, 1.62 Gs^{-1}, gain 500.

Singlet oxygen imaging by confocal laser scanning microscopy and image analysis. SOSG (Molecular Probes Inc. Eugene, OR, USA) was applied to the U266 cells in order to visualize $^1O_2$ production. Cell suspension treated with H_2O_2 was incubated with 50 µM SOSG for 30 min in dark. Following incubation, U266 cells were gently washed with 20 mM K-buffer, and consequently the $^1O_2$ imaging was performed by a confocal laser scanning microscope, Fluorview 1000 (Olympus Czech Group, Prague, Czech Republic). The transition images were obtained by transmitted light detection module with 405 nm excitation with a near-ultraviolet (UV) laser diode and Nomarski DIC filters (Olympus). Simultaneously visualized fluorescence channel resulted from excitation by a 488 nm line of argon laser, representing the signals for SOSG fluorescence detected by 505–525 nm emission filter set. The proper intensity of lasers was set according to unstained samples at the beginning of each experiment[54]. The integral distribution of signal intensity (ranging from 0 to 4095 levels of brightness) within the images was evaluated using software FV10-ASW 3.0 Viewer (Olympus).

1. Pospíšil, P. Molecular mechanisms of production and scavenging of reactive oxygen species by photosystem II. *Biochim. Biophys. Acta* **1817**, 218–231, doi:10.1016/j.bbabio.2011.05.017 (2012).
2. Han, D., Williams, E. & Cadenas, E. Mitochondrial respiratory chain-dependent generation of superoxide anion and its release into the intermembrane space. *Biochem. J.* **353**, 411–416, doi:10.1042/0264-6021:3530411 (2001).
3. Cocheme, H. M. & Murphy, M. P. Complex I is the major site of mitochondrial superoxide production by paraquat. *J. Biol. Chem.* **283**, 1786–1798, doi:10.1074/jbc.M708597200 (2008).
4. Dahlgren, C., Karlsson, A. & Bylund, J. Measurement of respiratory burst products generated by professional phagocytes. *Methods Mol. Biol.* **412**, 349–363, doi:10.1007/978-1-59745-467-4_23 (2007).
5. Gutteridge, J. M. C. Lipid-Peroxidation and Antioxidants as Biomarkers of Tissue-Damage. *Clin. Chem.* **41**, 1819–1828 (1995).
6. Halliwell, B. & Gutteridge, J. M. The definition and measurement of antioxidants in biological systems. *Free Radic. Biol. Med.* **18**, 125–126, doi:10.1016/0891-5849(95)91457-3 (1995).
7. Gutteridge, J. M. & Halliwell, B. Antioxidants: Molecules, medicines, and myths. *Biochem. Biophys. Res. Commun.* **393**, 561–564, doi:10.1016/j.bbrc.2010.02.071 (2010).
8. Dean, R. T., Gieseg, S. & Davies, M. J. Reactive Species and Their Accumulation on Radical-Damaged Proteins. *Trends Biochem. Sci.* **18**, 437–441, doi:10.1016/0968-0004(93)90145-D (1993).
9. Miyamoto, S. *et al*. Biological hydroperoxides and singlet molecular oxygen generation. *IUBMB Life* **59**, 322–331, doi:10.1080/15216540701242508 (2007).
10. Davies, M. J., Fu, S. L. & Dean, R. T. Protein Hydroperoxides Can Give Rise to Reactive Free-Radicals. *Biochem. J.* **305**, 643–649 (1995).
11. Cilento, G. & Nascimento, A. L. T. O. Generation of Electronically Excited Triplet Species at the Cellular-Level - a Potential Source of Genotoxicity. *Toxicol. Lett.* **67**, 17–28, doi:10.1016/0378-4274(93)90043-W (1993).
12. Darmanyan, A. P. & Foote, C. S. Definition of the Nature of Ketone Triplet-States on the Basis of Singlet Oxygen Generation Efficiency. *J. Phys. Chem.-Us* **97**, 4573–4576, doi:10.1021/J100120a003 (1993).
13. Cilento, G. & Adam, W. From free radicals to electronically excited species. *Free Radic. Biol. Med.* **19**, 103–114, doi:10.1016/0891-5849(95)00002-f (1995).
14. Pospíšil, P., Prasad, A. & Rác, M. Role of reactive oxygen species in ultra-weak photon emission in biological systems. *J. Photoch. Photobio. B* **139**, 11–23, doi:10.1016/j.jphotobiol.2014.02.008 (2014).
15. Adam, W., Bosio, S. G. & Turro, N. J. Highly diastereoselective dioxetane formation in the photooxygenation of enecarbamates with an oxazolidinone chiral auxiliary: Steric control in the [2 + 2] cycloaddition of singlet oxygen through conformational alignment. *J. Am. Chem. Soc.* **124**, 8814–8815, doi:10.1021/Ja026815k (2002).
16. Cilento, G. Excited electronic states in dark biological processes. *Q. Rev. Biophys.* **6**, 485–501 (1974).
17. Bechara, E. J. H., Oliveira, O., Duran, N., Debaptista, R. C. & Cilento, G. Peroxidase catalyzed generation of triplet acetone. *Photochem. Photobiol.* **30**, 101–110, doi:10.1111/j.1751-1097.1979.tb07121.x (1979).
18. Cilento, G. Generation of electronically excited triplet species in biochemical systems. *Pure Appl. Chem.* **56**, 1179–1190, doi:10.1351/pac198456091179 (1984).
19. Cilento, G., Debaptista, C. & Brunetti, I. L. Triplet Carbonyls from Photophysics to Biochemistry. *J. Mol. Struct.* **324**, 45–48, doi:10.1016/0022-2860(94)08225-1 (1994).
20. Mano, C. M. *et al*. Excited singlet molecular O-2 ((1)Delta g) is generated enzymatically from excited carbonyls in the dark. *Sci. Rep.* **4**, doi:10.1038/srep05938 (2014).
21. Wagner, P. in *Triplet States III* Vol. 66 *Top. Curr. Chem.* Ch. 1, 1–52 (Springer Berlin Heidelberg, 1976).
22. Sundquist, A. R., Hanusch, M., Stahl, W. & Sies, H. Cis-trans isomerization of carotenoids by the triplet carbonyl source 3-hydroxymethyl-3,4,4-trimethyl-1,2-dioxetane. *Photochem. Photobiol.* **57**, 785–791, doi:10.1111/j.1751-1097.1993.tb09211.x (1993).
23. Russell, G. A. Deuterium-Isotope Effects in the Autoxidation of Aralkyl Hydrocarbons - Mechanism of the Interaction of Peroxy Radicals. *J. Am. Chem. Soc.* **79**, 3871–3877, doi:10.1021/Ja01571a068 (1957).
24. Howard, J. A. & Ingold, K. U. Absolute rate constants for hydrocarbon autoxidation. V. The hydroperoxy radical in chain propagation and termination. *Can. J. Chemistry* **45**, 785–792, doi:10.1139/v67-131 (1967).
25. Miyamoto, S. *et al*. Linoleic acid hydroperoxide reacts with hypochlorous acid, generating peroxyl radical intermediates and singlet molecular oxygen. *Proc. Natl. Acad. Sci. U S A* **103**, 293–298, doi:10.1073/pnas.0508170103 (2006).
26. Miyamoto, S. *et al*. Linoleic acid hydroperoxide reacts with hypochlorite generating peroxyl radical intermediates and singlet oxygen. *Free Radic. Biol. Med.* **37**, S16–S16 (2004).
27. Miyamoto, S., Martinez, G. R., Medeiros, M. H. & Di Mascio, P. Singlet molecular oxygen generated from lipid hydroperoxides by the russell mechanism: studies using 18(O)-labeled linoleic acid hydroperoxide and monomol light emission measurements. *J. Am. Chem. Soc.* **125**, 6172–6179, doi:10.1021/ja029115o (2003).
28. Sun, S., Bao, Z., Ma, H., Zhang, D. & Zheng, X. Singlet oxygen generation from the decomposition of alpha-linolenic acid hydroperoxide by cytochrome c and lactoperoxidase. *Biochemistry* **46**, 6668–6673, doi:10.1021/bi700178u (2007).
29. Mendenhall, G. D., Sheng, X. C. & Wilson, T. Yields of Excited Carbonyl Species from Alkoxyl and from Alkylperoxyl Radical Dismutations. *J. Am. Chem. Soc.* **113**, 8976–8977, doi:10.1021/Ja00023a073 (1991).
30. Cifra, M. & Pospíšil, P. Ultra-weak photon emission from biological samples: Definition, mechanisms, properties, detection and applications. *J. Photoch. Photobio. B* **139**, 2–10, doi:10.1016/j.jphotobiol.2014.02.009 (2014).
31. Matsumoto, M. Advanced chemistry of dioxetane-based chemiluminescent substrates originating from bioluminescence. *J. Photoch. Photobio. C* **5**, 27–53, doi:10.1016/j.photochemrev.2004.02.001 (2004).

32. Timmins, G. S. *et al.* Lipid peroxidation-dependent chemiluminescence from the cyclization of alkylperoxyl radicals to dioxetane radical intermediates. *Chem. Res. Toxicol.* **10**, 1090–1096, doi:10.1021/tx970075p (1997).
33. Adam, W., Kazakov, D. V. & Kazakov, V. P. Singlet-oxygen chemiluminescence in peroxide reactions. *Chem. Rev.* **105**, 3371–3387, doi:10.1021/cr0300035 (2005).
34. Khan, A. U. in *In Singlet O_2* Vol. 1 (ed Frimer, A. A.) 39–79 (CRC Press, Boca Racon, FL 1985).
35. Flors, C. *et al.* Imaging the production of singlet oxygen in vivo using a new fluorescent sensor, Singlet Oxygen Sensor Green. *J. Exp. Bot.* **57**, 1725–1734, doi:10.1093/jxb/erj181 (2006).
36. Gollmer, A. *et al.* Singlet Oxygen Sensor Green (R): Photochemical Behavior in Solution and in a Mammalian Cell. *Photochem. Photobiol.* **87**, 671–679, doi:10.1111/j.1751-1097.2011.00900.x (2011).
37. Shen, Y. *et al.* Indirect imaging of singlet oxygen generation from a single cell. *Laser Phys. Lett.* **8**, 232–238, doi:10.1002/lapl.201010113 (2011).
38. Wei, S. H. *et al.* Synthesis and Type I/Type II photosensitizing properties of a novel amphiphilic zinc phthalocyanine. *Dyes Pigments* **71**, 61–67, doi:10.1016/j.dyepig.2005.06.016 (2006).
39. Bienert, G. P., Schjoerring, J. K. & Jahn, T. P. Membrane transport of hydrogen peroxide. *BBA-Biomembranes* **1758**, 994–1003, doi:10.1016/j.bbamem.2006.02.015 (2006).
40. Barbouti, A., Doulias, P. T., Zhu, B. Z., Frei, B. & Galaris, D. Intracellular iron, but not copper, plays a critical role in hydrogen peroxide-induced DNA damage. *Free Radic. Biol. Med.* **31**, 490–498, doi:10.1016/s0891-5849(01)00608-6 (2001).
41. Minisini, M. P., Kantengwa, S. & Polla, B. S. DNA-damage and stress protein-synthesis induced by oxidative stress proceed independently in the human premonocytic line U937. *Mutat. Res.-DNA Repair* **315**, 169–179, doi:10.1016/0921-8777(94)90016-7 (1994).
42. Hoffmann, M. E. & Meneghini, R. Action of hydrogen peroxide on human fibroblast in culture. *Photochem. Photobiol.* **30**, 151–155, doi:10.1111/j.1751-1097.1979.tb07128.x (1979).
43. Cadenas, E., Varsavsky, A. I., Boveris, A. & Chance, B. Oxygen- or organic hydroperoxide-induced chemiluminescence of brain and liver homogenates. *Biochem. J.* **198**, 645–654 (1981).
44. Cadenas, E., Boveris, A. & Chance, B. Spectral analysis of the low level chemiluminescence of H2O2-supplemented ferricytochrome c. *FEBS Lett.* **112**, 285–288, doi:10.1016/0014-5793(80)80199-2 (1980).
45. Cadenas, E., Arad, I. D., Boveris, A., Fisher, A. B. & Chance, B. Partial Spectral-Analysis of the Hydroperoxide-Induced Chemi-Luminescence of the Perfused Lung. *FEBS Lett.* **111**, 413–418, doi:10.1016/0014-5793(80)80839-8 (1980).
46. Hideg, E., Kobayashi, M. & Inaba, H. Spontaneous Ultraweak Light-Emission from Respiring Spinach Leaf Mitochondria. *Biochim. Biophys. Acta* **1098**, 27–31 (1991).
47. Mathew, B. G., Haorah, J. & Kumar, S. Weak Luminescence from Cotyledons of Cicer-Arietinum L Induced by Sudden Freezing and Thawing - the Role of Superoxide, Free-Radicals and Singlet Oxygen in the Phenomenon. *J. Photoch. Photobio. B* **16**, 297–304, doi:10.1016/1011-1344(92)80017-P (1992).
48. Takeda, M. *et al.* A novel method of assessing carcinoma cell proliferation by biophoton emission. *Cancer Lett.* **127**, 155–160, doi:10.1016/s0304-3835(98)00064-0 (1998).
49. Hall, R., Chamulitrat, W., Takahashi, N., Chignell, C. & Mason, R. Detection of Singlet oxygem phosphorescence during chloroperoxidase-catalyzed decomposition of ethyl hydroperoxide. *J. Biol. Chem.* **264**, 7900–7906 (1989).
50. Prado, F. M. *et al.* Thymine hydroperoxide as a potential source of singlet molecular oxygen in DNA. *Free Radic. Biol. Med.* **47**, 401–409, doi:10.1016/j.freeradbiomed.2009.05.001 (2009).
51. Uemi, M., Ronsein, G. E., Miyamoto, S., Medeiros, M. H. & Di Mascio, P. Generation of cholesterol carboxyaldehyde by the reaction of singlet molecular oxygen [O2 (1Delta(g))] as well as ozone with cholesterol. *Chem. Res. Toxicol.* **22**, 875–884, doi:10.1021/tx800447b (2009).
52. Niu, Q. J. & Mendenhall, G. D. Yields of Singlet Molecular-Oxygen from Peroxyl Radical Termination. *J. Am. Chem. Soc.* **114**, 165–172, doi:10.1021/Ja00027a024 (1992).
53. Kikuchi, J., Koyama, D., Mukai, H. Y. & Furukawa, Y. Suitable drug combination with bortezomib for multiple myeloma under stroma-free conditions and in contact with fibronectin or bone marrow stromal cells. *Int. J. Hematol.* **99**, 726–736, doi:10.1007/s12185-014-1573-3 (2014).
54. Sedlářová, M. *et al.* Influence of nitric oxide and reactive oxygen species on development of lettuce downy mildew in Lactuca spp. *Eur. J. Plant Pathol.* **129**, 267–280, doi:10.1007/s10658-010-9626-9 (2011).

Acknowledgments

This work was supported by the Ministry of Education, Youth and Sports of the Czech Republic through grants no. LO1204 (Sustainable development of research in the Centre of the Region Haná from the National Program of Sustainability I), no. CZ.1.07/2.3.00/20.0057 (Progress and Internationalization of Biophysical Research at the Faculty of Science, Palacký University), CZ.1.07/2.3.00/30.0004 (Support for Building Excellent Research Teams and Intersectoral Mobility at Palacký University), the Czech Science Foundation grant no. GP13-29294S, and IGA_PrF_2014001. We would like to thank Dr. Ankush Prasad for stimulating discussion.

Author contributions

P.P. and M.R. designed the study; M.R. performed most of the experiments; M.S. performed the experiments including confocal laser scanning microscopy, M.R. analyzed the data, P.P. and M.R. drafted the manuscript. All authors read and approved the final manuscript.

Additional information

Competing financial interests: The authors declare no competing financial interests.

How to cite this article: Rác, M., Sedlářová, M. & Pospíšil, P. The formation of electronically excited species in the human multiple myeloma cell suspension. *Sci. Rep.* **5**, 8882; DOI:10.1038/srep08882 (2015).